JACS
JOURNAL OF THE AMERICAN CHEMICAL SOCIETY
pubs.acs.org/JACS
Communication

Operando High-Energy-Resolution X-ray Spectroscopy of Evolving Cu Nanoparticle Electrocatalysts for CO_2 Reduction

Julian Feijóo, Yao Yang, Maria V. Fonseca Guzman, Alfred Vargas, Chubai Chen, Christopher J. Pollock, and Peidong Yang*

Cite This: *J. Am. Chem. Soc.* 2023, 145, 20208−20213
Read Online
ACCESS | Metrics & More | Article Recommendations | Supporting Information

ABSTRACT: Advances in electrocatalysis research rely heavily on building a thorough mechanistic understanding of catalyst active sites under realistic operating conditions. Only recently have techniques emerged that enable sensitive spectroscopic data collection to distinguish catalytically relevant surface sites from the underlying bulk material under applied potential in the presence of an electrolyte layer. Here, we demonstrate that *operando* high-energy-resolution fluorescence detected X-ray absorption spectroscopy (HERFD-XAS) is a powerful spectroscopic method which offers critical surface chemistry insights in CO_2 electroreduction with sub-electronvolt energy resolution using hard X-rays. Combined with the high surface area-to-volume ratio of 5 nm copper nanoparticles, *operando* HERFD-XAS allows us to observe with clear evidence the breaking of chemical bonds between the ligands and the Cu surface as part of the ligand desorption process occurring under electrochemical potentials relevant for the CO_2 reduction reaction (CO_2RR). In addition, the dynamic evolution of oxidation state and coordination number throughout the operation of the nanocatalyst was continuously tracked. With these results in hand, undercoordinated metallic copper nanograins are proposed to be the real active sites in the CO_2RR. This work emphasizes the importance of HERFD-XAS compared to routine XAS in catalyst characterization and mechanism exploration, especially in the complicated electrochemical CO_2RR.

To date, copper is the only element known to electrochemically convert CO_2 to valuable multicarbon products at appreciable rates. Detailed information about the local atomic scale structure of the involved active sites would help tackle the associated large overpotentials of around 1 V. It is well established that Cu nanocatalysts are highly mobile under CO_2 reduction reaction (CO_2RR) conditions, necessitating *operando* methods to characterize such systems under operating conditions.[1−3] Soft X-rays, while more sensitive to the catalytically relevant surface, are also more likely to cause beam-induced damage.[4] The limited penetration depth of soft X-rays requires thin-liquid configurations, which prevents bulk-level mass transport and can significantly affect the performance and structure of Cu catalysts.[5−8] The use of hard X-rays mitigates the oxidation of Cu, as shown by the reliable observation of metallic copper signals during CO_2RR.[9,10] In addition, the larger penetration depth removes the requirement for high vacuum and allows for the use of sufficient electrolyte volumes. To deconvolve information about the surface from hard X-ray measurements, it would be advantageous to reduce the background signal and increase energy resolution.

A promising technique that allows for such increased detail is high energy-resolution fluorescence detected (HERFD)-XAS.[11] In conventional fluorescence-mode XAS, the fluorescence signal is collected across a broad energy envelop (>100 eV), which in the hard X-ray regime results in a spectrum analogous to a transmission-mode spectrum,[12] with the broadening determined by the lifetime of the $1s^1$ excited state (1.0−1.6 eV for first row transition metals). In contrast, HERFD-XAS employs perfect crystal Bragg optics as energy analyzers to detect photons over a much narrower energy bandwidth (∼1 eV; Figure 1) with the lifetime broadening determined by the final $2p^5$ state of that decay channel rather than the intermediate $1s^1$ state (eq S1).[13] In this work, detection of the Cu $K_{\alpha 1}$ emission line results in an overall energy resolution of 0.66 eV when using a Si(311) monochromator, as compared to 1.6 eV for conventional XAS (eq S2). This enables the detection of even subtle features in the pre-edge region of XANES spectra, which are often obscured by the intense rising edge.

Detecting at a specific wavelength also greatly reduces the background signal relative to conventional XAS (Figures S1, S2).[14] In favorable cases, this can allow for the collection of data past other absorption edges.[15,16] The narrow energy bandwidth for detection coupled to the inherently smaller solid angle subtended by the crystal analyzers does have the effect of reducing the absolute count rate, though this can be mitigated by the high photon flux available from modern third generation synchrotron beamlines.

Based on the advantages discussed above, HERFD-XAS presents itself as a powerful technique to measure catalytically relevant properties. Notable examples in the recent literature include determination of substrate−metal interaction as the origin of strain in Pt nanoparticles[17] and identification of Fe

Received: July 31, 2023
Published: September 7, 2023

https://doi.org/10.1021/jacs.3c08182
J. Am. Chem. Soc. 2023, 145, 20208−20213

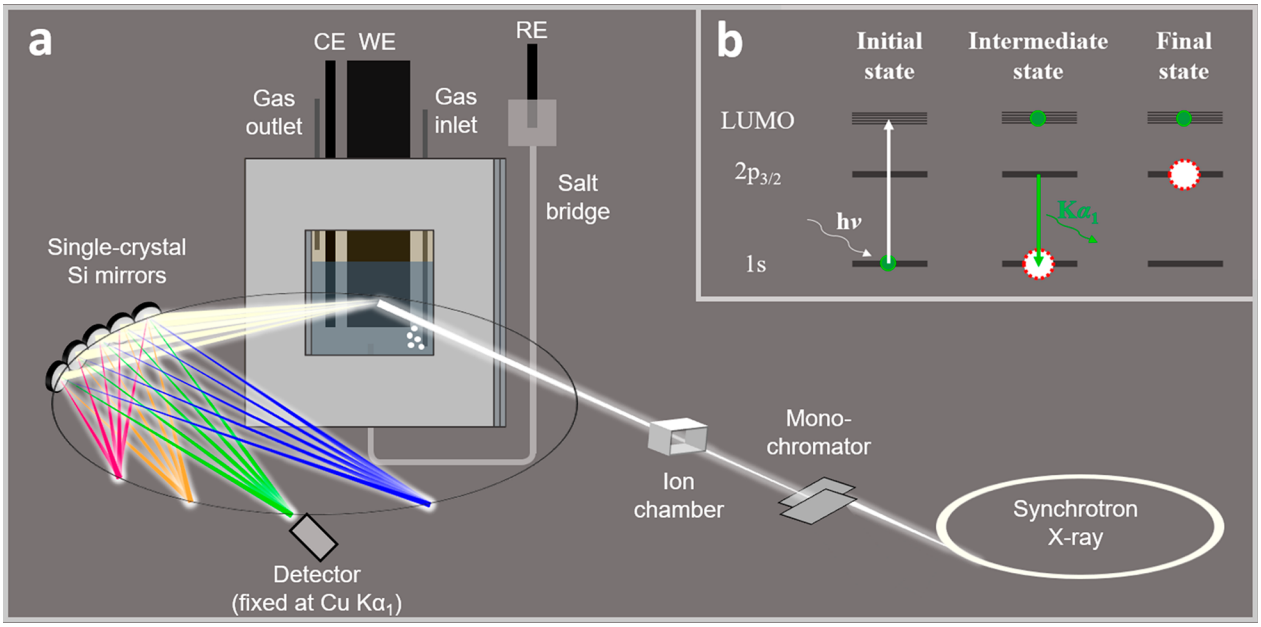

Figure 1. (a) Schematic showing the setup of the *operando* HERFD-XAS experiment. (b) Energy level diagram illustrating the involved electronic transitions.

atoms as the active sites of Co Fe oxygen evolution electrocatalysts.[18] To date, there are only a handful of studies using HERFD-XAS to study electrocatalysts *in operando*.[19−22] Of these, only one studied bulk Cu catalysts. Gao et al. used HERFD-XANES at a low incidence angle to characterize nanostructured Cu foil.[20] They observe a nearly complete reduction to metallic copper under the CO_2RR, although they report that iodide could stabilize small amounts of Cu^+. This work combines the high sensitivity of HERFD-XAS with a home-built *operando* electrochemical cell (Figure 1) to monitor highly active 5 nm Cu nanoparticles during CO_2RR.

To demonstrate the merit of HERFD-XAS, we study an electrocatalyst formed from an ensemble of 5 nm Cu nanoparticles, which to date is the most selective for desired C_{2+} products at low overpotential and neutral pH with a faradaic efficiency of 55% in an H-cell (Table S1).[23−25] Using a gas diffusion electrode would likely allow reaching industrially relevant current densities,[26] as we have shown for related 7 nm Cu nanoparticles.[25] Atomic-scale high-angle annular dark-field (HAADF) scanning transmission electron microscopy (STEM) images show a narrow size distribution of the pristine particles (Figure 2). The as-synthesized metallic particles quickly oxidize to polycrystalline cuprous oxide (Cu_2O) under ambient conditions. The high magnification image shows random orientations of the Cu_2O lattice fringes of a polycrystalline particle (Figure 1d). The tetradecylphosphonic acid (TDPA) ligands from the colloidal synthesis are not visible on the surface since HAADF-STEM imaging is more sensitive to heavier elements.

The dynamic evolution of the catalyst under CO_2RR conditions was then studied using *operando* HERFD-XAS in a home-built *operando* X-ray cell reported ealier.[27] Cyclic voltammetry of the catalyst in the X-ray cell shows comparable electrochemical behavior to that of a traditional H-cell (Figure S3). The decrease in the edge energy in the XANES region indicates the gradual transition from Cu_2O to metallic copper (Figure 3a). Because of the distinct shape and intensity in the pre-edge region of nanomaterials (Figure S4), the catalyst at

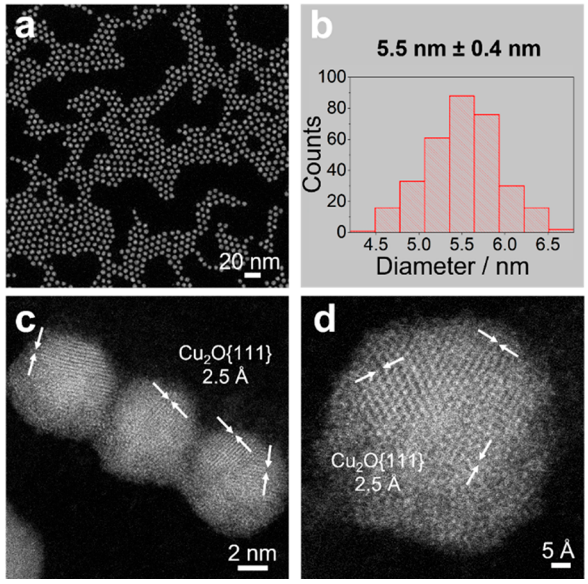

Figure 2. HAADF-STEM images of as-synthesized 5 nm Cu NPs. (a) Image showing closely packed nanoparticle ensembles. (b) Histogram showing the narrow particle size distribution. (c) Image showing Cu_2O lattice fringes. (d) High-magnification image of a single particle showing its polycrystalline nature.

the open circuit potential (OCP) and the steady-state catalyst were determined to be fully oxidized and fully metallic, respectively, by the close matching of their zero-crossings compared to bulk references in a second derivative plot (Figure S5). The transition to metallic Cu can also be observed from the appearance of the peak at around 9002 eV (Figure 3a). Linear combination fitting (LCF) was performed for a quantitative description of the oxidation state of Cu. Pristine particles and the steady-state catalyst were used as internal standards for Cu_2O and metallic Cu, respectively. The dashed lines in the magnified rising edge portion indicate the fitting range (Figure 3b). The LCF results show the rapidly

https://doi.org/10.1021/jacs.3c08182
J. Am. Chem. Soc. 2023, 145, 20208−20213

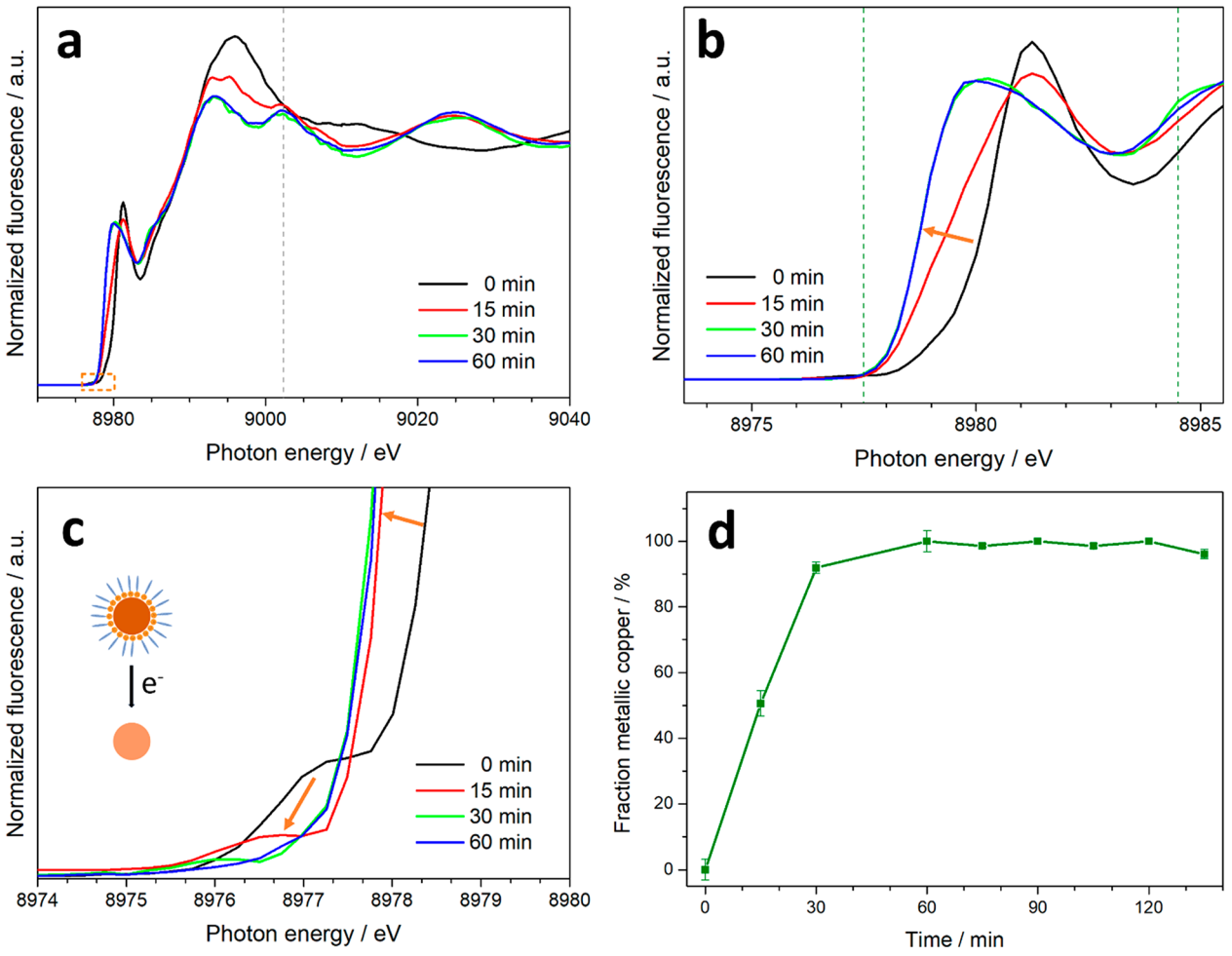

Figure 3. *Operando* HERFD-XANES characterization. (a) Overview of the XANES region showing the changing spectra with time. The dashed line shows the metallic feature around 9002 eV. (b) Magnification of the edge region showing reduction from Cu_2O to metallic Cu. The dashed green vertical lines indicate the linear combination fitting range. (c) Magnification of the ligand feature near 8977.2 eV, showing its fast decrease and eventual disappearance. (d) Results of the linear combination fitting, showing that the oxide catalyst is significantly reduced after just 30 min and fully metallic after 60 min of operation.

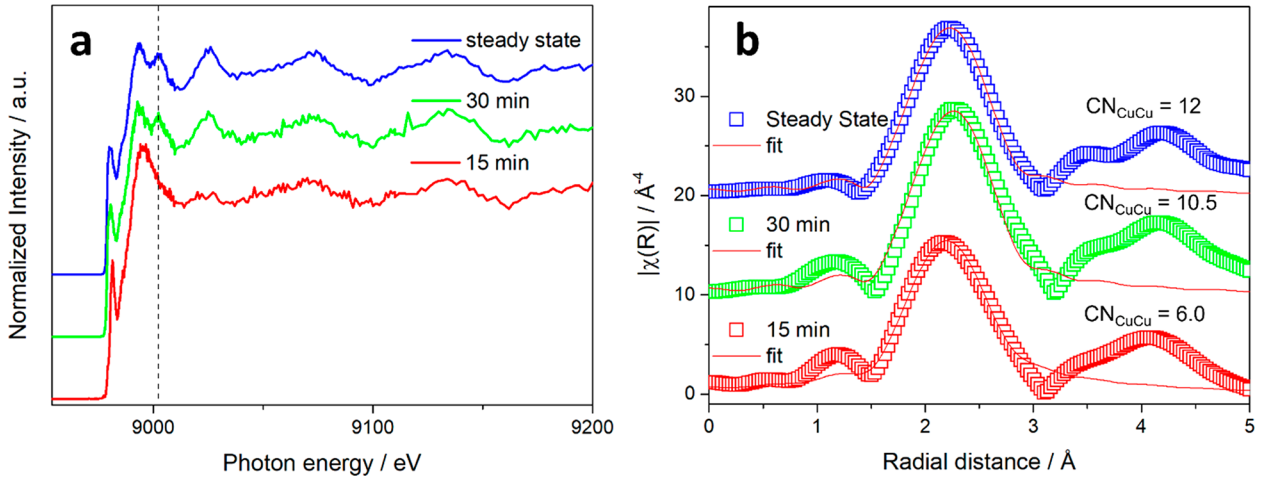

Figure 4. (a) Full XAS spectra after different times of electrolysis with dashed lines showing a metallic Cu feature at ~9002 eV emerging under CO_2RR and (b) corresponding Fourier-transformed EXAFS with fits in the R space.

decreasing amount of oxide from 100% at the OCP to 49% after 15 min and 8% after 30 min of applied potential at −0.8 V vs RHE (Figure 3d). After 1 h, the catalyst is fully metallic with a high-quality LCF fitting (reduced χ^2 = 0.000045). We conclude that metallic Cu nanograin active sites are responsible for our high C_2H_4 production and acknowledge that Cu oxide may exist when different Cu precursors and experimental conditions are used.[28]

https://doi.org/10.1021/jacs.3c08182
J. Am. Chem. Soc. 2023, 145, 20208−20213

The higher energy resolution of HERFD-XAS becomes apparent in the energy range just below the intense absorption edge features (Figure 3c). Here, an additional weak pre-edge absorption feature with less than 1% of the normalized intensity can be observed at around 8977.2 eV, which is not resolvable in conventional XAS (Figure S1). This feature occurs around 0.5 eV lower than the quadrupole-allowed transition of CuO (Figure S6). In addition, the rising edge matches our Cu-TDPA reference complex rather than Cu_2O or CuO, allowing us to assign it to ligand-modulated 3d−4p mixing due to the presence of the TDPA ligand at the surface of the pristine nanoparticles. The ligand-peak rapidly decreases in intensity under applied potential and is not visible in the steady state, indicating the complete detachment of the ligands from the Cu surface. The simultaneous slight energy shift of this pre-edge is potentially due to varying binding modes of the phosphonic acid headgroup; further investigations are underway. Removal of the protective ligand shell enables subsequent aggregation of the nanoparticles, as discussed below.

Further insights into the dynamic evolution of the catalyst under bias were obtained from EXAFS fitting (Figure 4b). Additional fitting information can be found in Figure S7, Discussions S1 and S2, and Tables S2−S6. After just 15 min, the R-space spectrum already looks mostly metallic. LCF of the pre-edge indicated around 50% of oxide phase at this time; the discrepancy results from the EXAFS region with metallic Cu being scanned later compared to the XANES region with residual oxide (Figure S8). This leaves more time for reduction to occur before the EXAFS region is scanned. The Cu−Cu coordination number (CN) of metallic copper increases throughout the dynamic evolution of the catalyst from 6.0 after 15 min to 10.5 after 30 min to 12.0 after 1 h. The intermediate state at 15 min represents a snapshot of the active state before the EXAFS becomes dominated by the larger Cu aggregates formed in the later stages of the catalyst's life cycle (Figure S9). The expected CN based on the nanoparticle size can be calculated (Discussion S2). In short, by taking into consideration the surface CN and fraction of surface atoms as a function of size,[29] an average CN of 11.2 is expected for 5 nm Cu NPs. The much lower CNs measured for the intermediate state suggest the presence of undercoordinated Cu surface sites, which have previously been reported to facilitate CO−CO coupling and thus lead to a larger multicarbon selectivity.[30−32] It should be noted that quantification of CN from EXAFS typically has an error bar of around 20%.[33]

The increasing average CN as a result of aggregation reflects a decrease in the surface-area-to-volume ratio and implies a decrease in the fraction of undercoordinated surface sites. It should be noted that selectivity toward the major C_{2+} product C_2H_4 increases on a similar time scale as the increase in CN (Figure S10). By itself, an aggregation-induced decrease in electrochemically active surface area (ECSA) would lead to a decreased activity, which in turn is expected to decrease local pH due to the reduced consumption of protons. C_2H_4 is reported to be more easily formed at high pH,[34] so this cannot be the dominant effect. Rather, we hypothesize that the buildup of reaction intermediates over the course of the electrolysis is responsible for increased C_2H_4 production: We have previously identified the formation of a CO reservoir near the surface of Cu electrocatalysts as essential for the downstream formation of multicarbon products.[35] Both Cu foil and Cu nanoparticles exhibited a significant increase in C_2H_4 formation only after a certain threshold concentration of CO in this reservoir was reached.[35] Cu nanoparticles reached this threshold at a less negative potential compared with Cu foil, explaining their increased C_2H_4 selectivity. We hypothesize that the aggregation of Cu nanoparticles leads to the formation of Cu nanograins, which efficiently trap CO near the surface. The increasing C_2H_4 selectivity in the initial stage of electrolysis is likely a result of the gradual buildup of this CO reservoir.

In summary, we used HERFD-XAS to collect both XANES and EXAFS spectra throughout the life cycle of a highly active Cu nanocatalyst under operating conditions. The high energy resolution has allowed us to unravel the activation mechanisms of the catalyst after application of electrochemical potentials, which involves the detachment of surface-bound ligands and the evolution of the oxidation state and coordination environment of the Cu surface. The pristine nanocatalysts were finally reduced to metallic Cu nanograins with undercoordinated active sites. The fully active state is reached after around 1 h; at this point, no residual oxide or bound ligands are present in the system.

This work highlights the technical advantage of HERFD-XAS regarding the analysis of surface properties, such as metal−ligand bonds. Observation of a variety of other catalytically relevant properties, such as substrate−metal interactions and metal−adsorbate interactions, is well within the scope of this technique. Moreover, the ability to measure element-specific EXAFS even when overlapping absorption edges are present allows for structural investigation of multimetallic electrocatalysts. Given all of these advantages, we anticipate that this technique will become an important part of the toolkit of the catalysis community to obtain detailed information about catalysts in their active state.

■ ASSOCIATED CONTENT

Supporting Information

The Supporting Information is available free of charge at https://pubs.acs.org/doi/10.1021/jacs.3c08182.

Experimental Section, Figures S1−S10, Tables S1−S6, eqs S1 and S2, and Discussion S1 and S2 (PDF)

■ AUTHOR INFORMATION

Corresponding Author

Peidong Yang − *Department of Chemistry, University of California, Berkeley, California 94720, United States; Chemical Sciences Division, Lawrence Berkeley National Laboratory, Berkeley, California 94720, United States; Department of Materials Science and Engineering, University of California, Berkeley, California 94720, United States; Kavli Energy NanoScience Institute, Berkeley, California 94720, United States;* orcid.org/0000-0003-4799-1684; Email: p_yang@berkeley.edu

Authors

Julian Feijóo − *Department of Chemistry, University of California, Berkeley, California 94720, United States; Chemical Sciences Division, Lawrence Berkeley National Laboratory, Berkeley, California 94720, United States*

Yao Yang − *Department of Chemistry, University of California, Berkeley, California 94720, United States; Chemical Sciences Division, Lawrence Berkeley National Laboratory, Berkeley, California 94720, United States; Miller Institute for Basic Research in Science, University of*

California, Berkeley, California 94720, United States; orcid.org/0000-0003-0321-3792

Maria V. Fonseca Guzman − *Department of Chemistry, University of California, Berkeley, California 94720, United States; Chemical Sciences Division, Lawrence Berkeley National Laboratory, Berkeley, California 94720, United States*

Alfred Vargas − *Department of Chemical and Biomolecular Engineering, University of California, Berkeley, California 94720, United States*

Chubai Chen − *Department of Chemistry, University of California, Berkeley, California 94720, United States; Chemical Sciences Division, Lawrence Berkeley National Laboratory, Berkeley, California 94720, United States;* orcid.org/0000-0003-2513-2707

Christopher J. Pollock − *Cornell High Energy Synchrotron Source, Cornell University, Ithaca, New York 14853, United States;* orcid.org/0000-0001-5736-513X

Complete contact information is available at: https://pubs.acs.org/10.1021/jacs.3c08182

Notes

The authors declare no competing financial interest.

■ ACKNOWLEDGMENTS

This work was supported by the Director, Office of Science, Office of Basic Energy Sciences, Chemical Sciences, Geosciences and Biosciences Division of the U.S. Department of Energy under Contract DE-AC02- 05CH11231, FWP CH030201 (Catalysis Research Program). This work is based on research conducted at the Center for High-Energy X-ray Sciences (CHEXS), which is supported by the National Science Foundation (BIO, ENG, and MPS Directorates) under award DMR-1829070. This work made use of TEM facilities at the CCMR which are supported through the National Science Foundation Materials Research Science and Engineering Center (NSF MRSEC) program (DMR-1719875). This work also used TEM facilities at the Molecular Foundry supported by the Office of Science, Office of Basic Energy Sciences, of the U.S. Department of Energy under Contract No. DE-AC02-05CH11231. Y.Y. acknowledges the support from the Miller Research Fellowship.

■ REFERENCES

(1) Timoshenko, J.; Roldan Cuenya, B. In Situ/Operando Electrocatalyst Characterization by X-Ray Absorption Spectroscopy. *Chem. Rev.* **2021**, *121*, 882−961.

(2) Lin, S.-C.; Chang, C.-C.; Chiu, S.-Y.; Pai, H.-T.; Liao, T.-Y.; Hsu, C.-S.; Chiang, W.-H.; Tsai, M.-K.; Chen, H. M. Operando Time-Resolved X-Ray Absorption Spectroscopy Reveals the Chemical Nature Enabling Highly Selective CO2 Reduction. *Nat. Commun.* **2020**, *11*, 3525.

(3) Zhu, Y.; Wang, J.; Chu, H.; Chu, Y.-C.; Chen, H. M. In Situ/Operando Studies for Designing Next-Generation Electrocatalysts. *ACS Energy Lett.* **2020**, *5*, 1281−1291.

(4) Yang, Y.; Roh, I.; Louisia, S.; Chen, C.; Jin, J.; Yu, S.; Salmeron, M. B.; Wang, C.; Yang, P. Operando Resonant Soft X-Ray Scattering Studies of Chemical Environment and Interparticle Dynamics of Cu Nanocatalysts for CO2 Electroreduction. *J. Am. Chem. Soc.* **2022**, *144*, 8927−8931.

(5) Somerville, S. V.; O'Mara, P. B.; Benedetti, T. M.; Cheong, S.; Schuhmann, W.; Tilley, R. D.; Gooding, J. J. Nanoconfinement Allows a Less Active Cascade Catalyst to Produce More C 2+ Products in Electrochemical CO2 Reduction. *J. Phys. Chem. C* **2023**, *127*, 289−299.

(6) Gunathunge, C. M.; Li, X.; Li, J.; Hicks, R. P.; Ovalle, V. J.; Waegele, M. M. Spectroscopic Observation of Reversible Surface Reconstruction of Copper Electrodes under CO 2 Reduction. *J. Phys. Chem. C* **2017**, *121*, 12337−12344.

(7) Eren, B.; Zherebetskyy, D.; Patera, L. L.; Wu, C. H.; Bluhm, H.; Africh, C.; Wang, L.-W.; Somorjai, G. A.; Salmeron, M. Activation of Cu(111) Surface by Decomposition into Nanoclusters Driven by CO Adsorption. *Science* **2016**, *351*, 475−478.

(8) Kim, Y.-G.; Baricuatro, J. H.; Javier, A.; Gregoire, J. M.; Soriaga, M. P. The Evolution of the Polycrystalline Copper Surface, First to Cu(111) and Then to Cu(100), at a Fixed CO2RR Potential: A Study by Operando EC-STM. *Langmuir* **2014**, *30*, 15053−15056.

(9) Dutta, A.; Rahaman, M.; Hecker, B.; Drnec, J.; Kiran, K.; Zelocualtecatl Montiel, I.; Jochen Weber, D.; Zanetti, A.; Cedeño López, A.; Martens, I.; Broekmann, P.; Oezaslan, M. CO2 Electrolysis - Complementary Operando XRD, XAS and Raman Spectroscopy Study on the Stability of CuxO Foam Catalysts. *J. Catal.* **2020**, *389*, 592−603.

(10) Suen, N.-T.; Kong, Z.-R.; Hsu, C.-S.; Chen, H.-C.; Tung, C.-W.; Lu, Y.-R.; Dong, C.-L.; Shen, C.-C.; Chung, J.-C.; Chen, H. M. Morphology Manipulation of Copper Nanocrystals and Product Selectivity in the Electrocatalytic Reduction of Carbon Dioxide. *ACS Catal.* **2019**, *9*, 5217−5222.

(11) Hämäläinen, K.; Siddons, D. P.; Hastings, J. B.; Berman, L. E. Elimination of the Inner-Shell Lifetime Broadening in x-Ray-Absorption Spectroscopy. *Phys. Rev. Lett.* **1991**, *67*, 2850−2853.

(12) De Groot, F. M. F.; Arrio, M. A.; Sainctavit, Ph.; Cartier, Ch.; Chen, C. T. Fluorescence Yield Detection: Why It Does Not Measure the X-Ray Absorption Cross Section. *Solid State Commun.* **1994**, *92*, 991−995.

(13) Glatzel, P.; Bergmann, U. High Resolution 1s Core Hole X-Ray Spectroscopy in 3d Transition Metal Complexes—Electronic and Structural Information. *Coord. Chem. Rev.* **2005**, *249*, 65−95.

(14) Cutsail, G. E.; Banerjee, R.; Zhou, A.; Que, L.; Lipscomb, J. D.; DeBeer, S. High-Resolution Extended X-Ray Absorption Fine Structure Analysis Provides Evidence for a Longer Fe···Fe Distance in the Q Intermediate of Methane Monooxygenase. *J. Am. Chem. Soc.* **2018**, *140*, 16807−16820.

(15) Yano, J.; Pushkar, Y.; Glatzel, P.; Lewis, A.; Sauer, K.; Messinger, J.; Bergmann, U.; Yachandra, V. High-Resolution Mn EXAFS of the Oxygen-Evolving Complex in Photosystem II: Structural Implications for the Mn4Ca Cluster. *J. Am. Chem. Soc.* **2005**, *127*, 14974−14975.

(16) Lafuerza, S.; Retegan, M.; Detlefs, B.; Chatterjee, R.; Yachandra, V.; Yano, J.; Glatzel, P. New Reflections on Hard X-Ray Photon-in/Photon-out Spectroscopy. *Nanoscale* **2020**, *12*, 16270−16284.

(17) Frenkel, A. I.; Small, M. W.; Smith, J. G.; Nuzzo, R. G.; Kvashnina, K. O.; Tromp, M. An in Situ Study of Bond Strains in 1 Nm Pt Catalysts and Their Sensitivities to Cluster-Support and Cluster-Adsorbate Interactions. *J. Phys. Chem. C* **2013**, *117*, 23286−23294.

(18) Hung, S.-F.; Chan, Y.-T.; Chang, C.-C.; Tsai, M.-K.; Liao, Y.-F.; Hiraoka, N.; Hsu, C.-S.; Chen, H. M. Identification of Stabilizing High-Valent Active Sites by Operando High-Energy Resolution Fluorescence-Detected X-Ray Absorption Spectroscopy for High-Efficiency Water Oxidation. *J. Am. Chem. Soc.* **2018**, *140*, 17263−17270.

(19) Friebel, D.; Louie, M. W.; Bajdich, M.; Sanwald, K. E.; Cai, Y.; Wise, A. M.; Cheng, M.-J.; Sokaras, D.; Weng, T.-C.; Alonso-Mori, R.; Davis, R. C.; Bargar, J. R.; Nørskov, J. K.; Nilsson, A.; Bell, A. T. Identification of Highly Active Fe Sites in (Ni,Fe)OOH for Electrocatalytic Water Splitting. *J. Am. Chem. Soc.* **2015**, *137*, 1305−1313.

(20) Gao, D.; Sinev, I.; Scholten, F.; Arán-Ais, R. M.; Divins, N. J.; Kvashnina, K.; Timoshenko, J.; Roldan Cuenya, B. Selective CO 2 Electroreduction to Ethylene and Multicarbon Alcohols via Electro-

lyte-Driven Nanostructuring. Angew. *Chem.* **2019**, *131*, 17203−17209.
(21) Bai, L.; Hsu, C.-S.; Alexander, D. T. L.; Chen, H. M.; Hu, X. Double-Atom Catalysts as a Molecular Platform for Heterogeneous Oxygen Evolution Electrocatalysis. *Nat. Energy* **2021**, *6*, 1054−1066.
(22) Chen, P.-C.; Chen, C.; Yang, Y.; Maulana, A. L.; Jin, J.; Feijoo, J.; Yang, P. Chemical and Structural Evolution of AgCu Catalysts in Electrochemical CO2 Reduction. *J. Am. Chem. Soc.* **2023**, *145*, 10116−10125.
(23) Kim, D.; Kley, C. S.; Li, Y.; Yang, P. Copper Nanoparticle Ensembles for Selective Electroreduction of CO 2 to C 2 -C 3 Products. *Proc. Natl. Acad. Sci. U. S. A.* **2017**, *114* (40), 10560−10565.
(24) Li, Y.; Kim, D.; Louisia, S.; Xie, C.; Kong, Q.; Yu, S.; Lin, T.; Aloni, S.; Fakra, S. C.; Yang, P. Electrochemically Scrambled Nanocrystals Are Catalytically Active for CO 2 -to-Multicarbons. *Proc. Natl. Acad. Sci. U.S.A.* **2020**, *117*, 9194−9201.
(25) Yang, Y.; Louisia, S.; Yu, S.; Jin, J.; Roh, I.; Chen, C.; Fonseca Guzman, M. V.; Feijóo, J.; Chen, P.-C.; Wang, H.; Pollock, C. J.; Huang, X.; Shao, Y.-T.; Wang, C.; Muller, D. A.; Abruña, H. D.; Yang, P. Operando Studies Reveal Active Cu Nanograins for CO2 Electroreduction. *Nature* **2023**, *614*, 262−269.
(26) Zheng, M.; Wang, P.; Zhi, X.; Yang, K.; Jiao, Y.; Duan, J.; Zheng, Y.; Qiao, S.-Z. Electrocatalytic CO 2 -to-C 2+ with Ampere-Level Current on Heteroatom-Engineered Copper via Tuning *CO Intermediate Coverage. *J. Am. Chem. Soc.* **2022**, *144*, 14936−14944.
(27) Yang, Y.; Wang, Y.; Xiong, Y.; Huang, X.; Shen, L.; Huang, R.; Wang, H.; Pastore, J. P.; Yu, S.-H.; Xiao, L.; Brock, J. D.; Zhuang, L.; Abruña, H. D. In Situ X-Ray Absorption Spectroscopy of a Synergistic Co-Mn Oxide Catalyst for the Oxygen Reduction Reaction. *J. Am. Chem. Soc.* **2019**, *141*, 1463−1466.
(28) Li, H.; Jiang, Y.; Li, X.; Davey, K.; Zheng, Y.; Jiao, Y.; Qiao, S.-Z. C 2+ Selectivity for CO 2 Electroreduction on Oxidized Cu-Based Catalysts. *J. Am. Chem. Soc.* **2023**, *145*, 14335−14344.
(29) Reske, R.; Mistry, H.; Behafarid, F.; Roldan Cuenya, B.; Strasser, P. Particle Size Effects in the Catalytic Electroreduction of CO 2 on Cu Nanoparticles. *J. Am. Chem. Soc.* **2014**, *136*, 6978−6986.
(30) Li, J.; Che, F.; Pang, Y.; Zou, C.; Howe, J. Y.; Burdyny, T.; Edwards, J. P.; Wang, Y.; Li, F.; Wang, Z.; De Luna, P.; Dinh, C.-T.; Zhuang, T.-T.; Saidaminov, M. I.; Cheng, S.; Wu, T.; Finfrock, Y. Z.; Ma, L.; Hsieh, S.-H.; Liu, Y.-S.; Botton, G. A.; Pong, W.-F.; Du, X.; Guo, J.; Sham, T.-K.; Sargent, E. H.; Sinton, D. Copper Adparticle Enabled Selective Electrosynthesis of N-Propanol. *Nat. Commun.* **2018**, *9*, 4614.
(31) Baturina, O. A.; Lu, Q.; Padilla, M. A.; Xin, L.; Li, W.; Serov, A.; Artyushkova, K.; Atanassov, P.; Xu, F.; Epshteyn, A.; Brintlinger, T.; Schuette, M.; Collins, G. E. CO2 Electroreduction to Hydrocarbons on Carbon-Supported Cu Nanoparticles. *ACS Catal.* **2014**, *4*, 3682−3695.
(32) Tang, W.; Peterson, A. A.; Varela, A. S.; Jovanov, Z. P.; Bech, L.; Durand, W. J.; Dahl, S.; Nørskov, J. K.; Chorkendorff, I. The Importance of Surface Morphology in Controlling the Selectivity of Polycrystalline Copper for CO2 Electroreduction. *Phys. Chem. Chem. Phys.* **2012**, *14*, 76−81.
(33) Abruna, H. D.; White, J. H.; Albarelli, M. J.; Bommarito, G. M.; Bedzyk, M. J.; McMillan, M. Is There Any Beam yet? Uses of Synchrotron Radiation in the in Situ Study of Electrochemical Interfaces. *J. Phys. Chem.* **1988**, *92*, 7045−7052.
(34) Wang, L.; Nitopi, S. A.; Bertheussen, E.; Orazov, M.; Morales-Guio, C. G.; Liu, X.; Higgins, D. C.; Chan, K.; Nørskov, J. K.; Hahn, C.; Jaramillo, T. F. Electrochemical Carbon Monoxide Reduction on Polycrystalline Copper: Effects of Potential, Pressure, and PH on Selectivity toward Multicarbon and Oxygenated Products. *ACS Catal.* **2018**, *8*, 7445−7454.
(35) Louisia, S.; Kim, D.; Li, Y.; Gao, M.; Yu, S.; Roh, I.; Yang, P. The Presence and Role of the Intermediary CO Reservoir in Heterogeneous Electroreduction of CO2. *Proc. Natl. Acad. Sci. U.S.A.* **2022**, *119*, No. e2201922119.

https://doi.org/10.1021/jacs.3c08182
J. Am. Chem. Soc. 2023, 145, 20208−20213